Nanoparticles from Lipid-Based Liquid Crystals: Emulsifier Influence on Morphology and Cytotoxicity

Sergio Murgia,[†] Angela M. Falchi,[‡] Miguel Mano,[§] Sandrina Lampis,[†] Rossella Angius,[†] Anna M. Carnerup,[||] Judith Schmidt,[⊥] Giacomo Diaz,[‡] Mauro Giacca,[§] Yeshayahu Talmon,[⊥] and Maura Monduzzi*[,†]

Department of Chemical Science, Cagliari University, CNBS and CSGI, ss 554, bivio Sestu, 09042 Monserrato (CA), Italy, Department of Cytomorphology, Cagliari University, ss 554, bivio Sestu, 09042 Monserrato (CA), Italy, Molecular Medicine Laboratory, International Centre for Genetic Engineering and Biotechnology (ICGEB), Padriciano 99, 34012 Trieste, Italy, Physical Chemistry 1, Center for Chemistry and Chemical Engineering, Lund University, P.O. Box 124, SE-221 00 Lund, Sweden, and Department of Chemical Engineering, Technion—Israel Institute of Technology, Haifa 32000, Israel

Received: October 14, 2009; Revised Manuscript Received: January 29, 2010

Here, monoolein-based nanoparticles (NPs), obtained through fragmentation of bulk liquid crystalline phases, and stabilized by two different emulsifiers, namely, Pluronic F127 (PF127) and lauroylcholine chloride (LCh), are investigated for structural features and for short-term in vitro cytotoxicity. Depending on the emulsifiers, different morphologies of the lipid NPs (cubosomes and liposomes) are obtained, as demonstrated by cryo-TEM images. Although NPs offer many advantages in medical applications and various chemicals used for their preparation are under investigation, so far there are no standardized procedures to evaluate cell biocompatibility. Two different protocols to evaluate the impact of these lipid NPs on biological systems are presented. Results show that nanoparticles stabilized by PF127 (cubosomes) display a relevant toxicity toward different cell lines, whereas those stabilized by LCh (liposomes) affect cell viability at a much lesser extent.

Introduction

Nanotoxicology is a topic of increasing and widespread interest due to the paradigm shift generated by the innovative performance of nanomaterials in many different fields.[1−5] Particularly, in the nanomedicine area,[6] the lack of simple but specific and validated protocols to evaluate the impact of nanomaterials and nanoparticles on biological systems is limiting practical applications.

The peculiar self-assembly features of lipids suggest wider exploitation of these systems to produce functionalized formulations that may retain important similarities and affinity toward biological membranes. Molecular recognition, bioadhesion, and self-assembly are crucial phenomena in several biological processes.[7−10] In particular, understanding the interactions between nanoparticles and biological membranes is of utmost importance in drug delivery applications. The ultimate goal, in this case, is to localize nano-objects at the desired position, thus favoring a specific interaction. For instance, it has been demonstrated that self-assembly properties lead to an increased bioadhesion in drug delivery systems based on surface active lipids.[11,12] These properties are basically established by the (effective) geometric features of the involved molecules, and of their self-assembly nanostructures.[13,14]

Nowadays, there is sufficient awareness that nanosized materials may show an increased and/or diverse interaction toward biological entities, thus developing toxicity. Eventual toxicological effects[1−4,15,16] are related to the dimension of the nanoparticles, which determines the available surface area, and to the specific interactions, which are responsible for molecular recognition. Recently, different effects have been recorded upon changing either experimental conditions or cell lines.[5] Therefore, when dealing with nanoparticles in solution, beyond the role of the nanosize that favors bioadhesion, the chemical nature of the involved surfaces is of paramount importance. Natural lipids constitute a class of molecules that appear to be a good starting point to prepare biocompatible drug delivery formulations.[12,17]

Since the extensive pioneering work of K. Larsson[18,19] in which the monoolein (MO) phase behavior in water (W) was clarified, and found to mimic membrane features, several studies have investigated the possible use of MO based systems for drug delivery.[11] In the MO/W system, the existence of two types of bicontinuous cubic liquid crystalline (LC) phases, namely, the gyroid (C_G, Ia3d space group) and the diamond (C_D, Pn3m space group), is the most peculiar feature. Remarkably, the diamond C_D cubic phase can coexist with an excess of water.

Bicontinuous cubic phases consist of surfactant bilayers, the curvature of which is modulated along an infinite periodic minimal surface (IPMS) having cubic symmetry.[14,20,21] The three most important bicontinuous cubic structures that have been identified in lipids are the aforementioned C_G and C_D and the primitive (C_P, Im3m space group). Indeed, the presence of a lipid bilayer favors adhesion and molecular recognition,[8,9] whereas the occurrence of polar and apolar non-intersecting continuous domains allows for the solubilization of almost any type of drugs.[10,11] In addition, the stiffness of the cubic cell can protect the drug,[10,22,23] and allows for controlled release.[10,12]

In previous works, MO based cubic and reverse hexagonal LC phase systems were prepared as lipid nanoparticle (LNP)

* Corresponding author. Phone: +39070675438. Fax: +390706754388. E-mail: monduzzi@unica.it.
[†] Department of Chemical Science, Cagliari University.
[‡] Department of Cytomorphology, Cagliari University.
[§] International Centre for Genetic Engineering and Biotechnology (ICGEB).
[||] Lund University.
[⊥] Technion—Israel Institute of Technology.

10.1021/jp9098655
Published on Web 02/19/2010

dispersions stabilized by Pluronic F127 (PF127) as emulsifier.[17,24,25] Surprisingly, cryo-TEM (cryogenic-temperature transmission electron microscopy) and AFM (atomic force microscopy) have shown that this process generates nanoparticles of cubic (cubosomes) and hexagonal (hexosomes) shape.[25,26] Nonetheless, the intrinsic cubic or hexagonal nanostructure, as determined via ^{13}C NMR relaxation,[27] and SAXRD (small angle X-ray diffraction)[28] is retained.

Such formulations are commonly prepared using either a bottom-up or a top-down approach. The former is mainly accomplished by diluting and then homogenizing a liquid mixture of the emulsifier and MO in water (nanoparticles form by nucleation in the aqueous solution),[24,28,29] while the latter implies the fragmentation of a massive LC phase in an aqueous solution of the emulsifier.[30] The top-down approach allows, in principle, for the entrapment of hydrophilic drugs (oligonucleotides, peptides, and proteins) that, on the contrary, cannot be easily introduced when preparing the dispersions directly from the components as previously reported.[17,24,31]

This work focuses on the influence of the emulsifier in addressing morphological features and biocompatibility of LNPs prepared through direct fragmentation of a bulk cubic LC phase using a high-speed homogenizer. The kinetic stabilization of the dispersions is achieved through the use of Pluronic F127 (PF127), a nonionic triblock copolymer PEO−PPO−PEO based on polyethylene oxide (PEO) and polypropylene oxide (PPO), or lauroylcholine chloride (LCh), a short chain cationic surfactant. The morphology and the topology of the LNP dispersions were characterized by cryo-TEM,[32] while the structural arrangement of the interface was investigated via ^{13}C NMR relaxation techniques. The evaluation of the cytotoxicity was performed using different cell lines, namely, mouse 3T3 fibroblasts (M3T3), human epithelial cervical carcinoma (HeLA), and human embryonic kidney (HEK 293T), and two different procedures based on image analysis and on the modified Alamar Blue assay.

Experimental Methods

Chemicals. Monoolein (MO, 1-monooleoylglycerol, RYLO MG 90-glycerol monooleate; 98.1 wt % monoglyceride) was kindly provided by Danisco Ingredients, Brabrand, Denmark. Lauroylcholine chloride and Pluronic F127 ($PEO_{99}-PPO_{67}-PEO_{99}$) were from Sigma. Distilled water, passed through a Milli-Q water purification system (Millipore), was used to prepare the samples.

Sample Preparation. Cubic phases were prepared by weighing the appropriate amounts of components (MO and water) into glass tubes ($\varnothing \approx 0.5$ cm) that were immediately sealed, centrifuged at 3000 rpm at 25 °C, and allowed to equilibrate at 25 °C for 1 week.

Dispersions were prepared by adding into a water solution of PF127 or LCh an appropriate amount of cubic phase (MO/W = 70/30), which is subsequently fragmented by an Ultra-Turrax T10 (IKA), equipped with a S10N-5G dispersing tool, working at 30.000 rpm for 20 min. In all experiments, the total dispersed phase (LC + emulsifier) was 5 wt %, with 6 wt % of PF127 or LCh with respect to MO/W weight. The sample volume was usually 2.5 mL.

Small-Angle X-ray Diffraction. SAXRD patterns were recorded at 25 °C at the Austrian beamline (camera length 100 cm) at the synchrotron light source ELETTRA (Trieste, Italy), using a Gabriel-type 1D position sensitive detector containing 2048 channels, which covered a d-range much larger than that of interest (10−200 Å) at an energy of 8 keV ($\lambda = 1.54$ Å). Silver behenate ($CH_3-(CH_2)_{20}-COOAg$) with a d spacing value of 58.38 Å was used as a standard to calibrate the angular scale of the measured intensity. Experiments were performed using a few milligrams of the sample enclosed in a stainless steel sample holder with thin polymer sheet windows. The lattice parameter, a, of the cubic phases was determined using the relation $d = 1/s = (1/a)(h^2 + k^2 + l^2)^{1/2}$ from linear fits of the plots of s versus $(h^2 + k^2 + l^2)^{1/2}$, where s is the measured peak position and h, k, and l are the Miller indices.

Cryogenic-Transmission Electron Microscopy (Cryo-TEM). Vitrified specimens were prepared in a controlled environment vitrification system (CEVS), at 25 °C and 100% relative humidity. A drop of the sample was placed on a perforated carbon film-coated copper grid, blotted with filter paper, and plunged into liquid ethane at its freezing point. The vitrified specimens were transferred to an Oxford CT-3500 cooling holder, and observed at 120 kV acceleration voltage in an FEI T12 transmission electron microscope at about −180 °C in the low-dose imaging mode to minimize electron-beam radiation damage. Images were digitally recorded with a Gatan US1000 high-resolution CCD camera.

Cryo-TEM Images Analysis. Fast Fourier transform and sizing of the nanoparticles were performed by ImageJ 1.42p (NIH, USA) and Image-Pro Express 6.0 (Media Cybernetics, Inc.) software, respectively. The accuracy of the lattice parameter determined from cryo-TEM images analysis was estimated around ±10%.

NMR. ^{13}C NMR measurements were carried out by a Bruker Avance 300 MHz (7.05 T) spectrometer at an operating frequency of 75.475 MHz, at 25 °C. A standard variable temperature control unit (with an accuracy of 0.5 °C) was used. ^1H-decoupling was applied in all ^{13}C NMR experiments. Spin−lattice (T_1) relaxation rates were obtained by means of the usual inversion recovery (180−τ−90−acquisition) sequences. T_1 were obtained by a three-parameter nonlinear fit to eq 1 of the partially relaxed NMR signal intensities obtained at 14−18 different t values.

$$I(\tau) = A - B\exp(-\tau T_1) \quad (1)$$

Particularly, in relaxation time NMR experiments, the error on the fitting was always less than 1% (standard deviation). Errors in the NMR measurements are reported in terms of standard deviation measured over three different experiments for each sample.

Cell Cultures. Mouse Swiss 3T3 fibroblasts (ATCC collection), HeLa (human epithelial cervical carcinoma), and HEK 293T (human embryonic kidney) cell lines were grown in Dulbecco's modified Eagle's medium (DMEM, Gibco, Life Technologies, Grand Island, NY) with high glucose, supplemented with 10% (v/v) fetal bovine serum, penicillin (100 U mL^{-1}), and streptomycin (100 μg mL^{-1}) (Gibco) at 37 °C in a 5% (v/v) CO_2 incubator.

Image Analysis on 3T3 Cells. 3T3 cell lines were seeded in number of 10^5 cells/cm^2 in 35 mm glass-bottomed dishes (MatTek, Ashland, MA). One day after seeding, nanoparticle formulations were added to the cells in serum-free medium (to avoid aggregation with serum) at a concentration of 1:200 (10 μL of LNP formulations in 2 mL of cell growth medium). The incubation time was 1 h. After incubation, the cells were washed twice with PBS (to remove all nanoparticles); then, they were supravitally stained for 15 min with the following probes: 300 nM Nile Red (NR, Fluka, Buchs, SG, Switzerland) and 650 nM Hoechst 33258 (Sigma, St. Louis, MO). The excitation and emission filters for NR were as follows: ex 460 ± 25 nm, em 535 ± 20 nm (band-pass) for nonpolar lipids; ex 540 ± 12.5

nm, em >590 nm (long pass) for polar lipids. The excitation and emission filters for Hoechst 33258 were the following: ex 360 ± 20 nm, em 460 ± 25 nm. The adopted filters allowed for a virtually complete separation of the emission and simultaneous observation of the two probes in live cells. The vehicles were DMSO for NR and water for Hoechst 33258. Stock solutions were 1000-fold concentrated to not exceed the 0.1% vehicle concentration in the medium. All experiments were replicated three times.

Observations were made using an Olympus IX 71 inverted microscope (Olympus, Tokyo, Japan) with 20× (0.7 NA) and 60× (1.3 NA/oil immersion) planapochromatic objectives (UPlanSApo series). Images were taken with a 12-bit cooled CCD camera (Sensicam PCO, Kelheim, Germany), coupled to a mechanical shutter interposed between the 100 W Hg lamp and the microscope, to limit illumination of cells to the time strictly required for acquisition of images. Excitation light was attenuated with a 6% neutral density filter. Image analysis and measurements were performed with the ImagePro Plus package (Media Cybernetics, Silver Springs, MD).

In the case of LCh-stabilized NPs, internalization was proved by adding NR in the LC matrix before the dispersion process. The image analysis showed results very similar to those reported in Figure 5a.

Alamar Blue Assay on HeLa and HEK 293T Cells. For cell viability experiments, 0.3×10^5 cells/well were seeded onto 24-well plates, 24 h prior to incubation with the different formulations. Nanoparticle formulations were added to the cells in serum-free medium at a concentration of 1:200 (10 μL of LNP formulations in 2 mL of cell growth medium). Cell viability was assessed by a modified Alamar Blue assay. Viable cells cause the reduction of Alamar Blue dye, resulting in a chemical change from a blue form (resazurin) to a red form (resorufin). A decrease in cell viability is determined by a drop in the capacity of cells to reduce the resazurin present in the medium. Briefly, 4 h after incubation with the different formulations, cells were incubated with DMEM containing 10% (v/v) Alamar Blue dye (resazurin). After 1 h of incubation, the absorbance of the medium was measured at 540 and 630 nm. Cell viability was calculated, as a percentage of the untreated control cells, according to eq 2:

$$\text{cell viability (\% of control)} = \frac{(A_{540} - A_{630})}{(A'_{540} - A'_{630})} \times 100 \quad (2)$$

where A_{540} and A_{630} are the absorbances of the samples and A'_{540} and A'_{630} those of control cells, at the indicated wavelengths.

Statistical Analysis. All data are presented as mean ± standard deviation (SD). Data were analyzed using GraphPad Prism software. The statistical significance of differences between data (each experiment compared to the corresponding control) was evaluated by a two-tailed unpaired *t* test at a 95% confidence level ($p \leq 0.05$).

Results

Phase Behavior of the Bulk Liquid Crystalline Phase. Since polarity, shape, and concentration of additives may induce geometrical and topogical modifications on the MO/W system,[22,33] the consequence of the incorporation of both PF127 and LCh on the bulk cubic LC phases used to prepare the nanoparticle dispersion was investigated via SAXRD experiments (Figure 1). Consider the two emulsifiers under investigation: in water, PF127 (MW = 12 600) forms large micelles that are stabilized by an extensive solvation of the EO groups, while LCh (MW = 321.9) forms very small micelles stabilized by solvation and

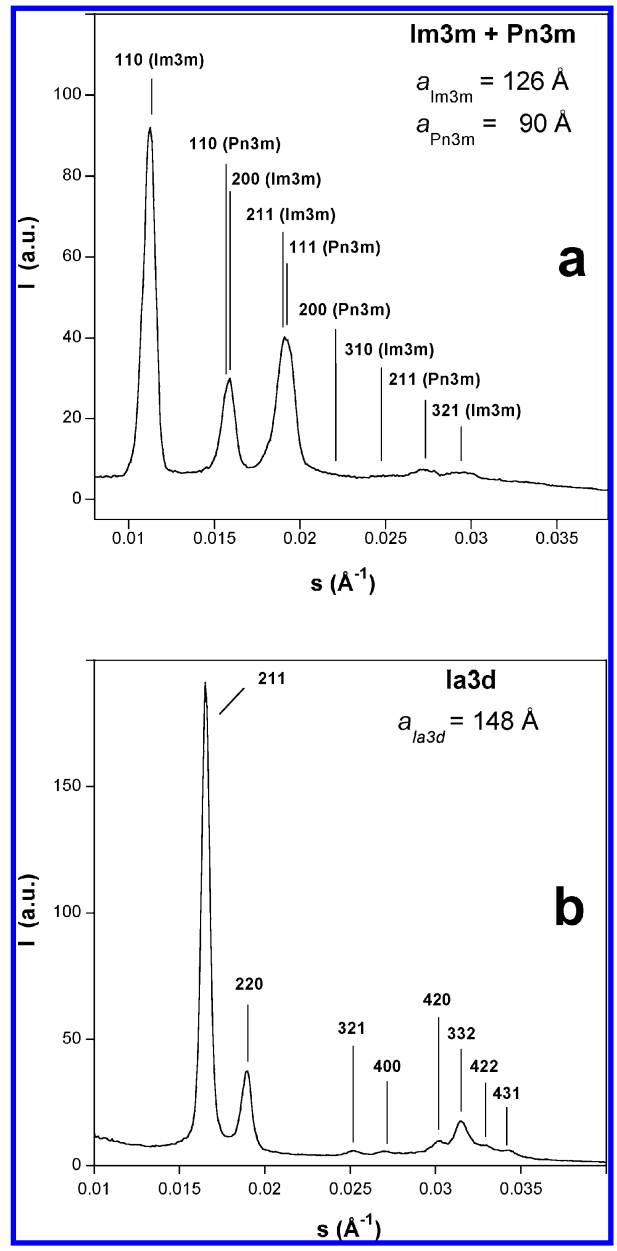

Figure 1. SAXRD patterns at 25 °C: (a) MO/W/PF127 (56.4/37.6/6.0 wt %) sample; (b) MO/W/LCh (60.1/36.9/3.0 wt %) sample. The Miller indices *hkl* are given for each reflection.

electrostatic interactions. A MO/W (70/30 w/w) system forms a C_G cubic phase.[21] In the presence of PF127 and in excess of water, the MO/W system evolves toward the C_D phase, coexisting with the C_P phase.[34] Figure 1a shows the SAXRD diffractogram of a MO/W/PF127 sample containing 6 wt % PF127 for which the expected combination of C_D (lattice parameter a = 90 Å) and C_P (lattice parameter a = 126 Å) nanostructures is identified. Conversely, the addition of 2−6 wt % LCh does not modify the original C_G phase, even in excess of water. The MO/W system in the presence of 3 wt % LCh shows a large region of lamellar phase (L_α) in the range 2−18 wt % of water, a $L_\alpha + C_G$ two-phase region in the range 18−32 wt % of water, and a pure C_G phase for water content greater than 32 wt %. Figure 1b shows the C_G SAXRD pattern of a MO/W sample containing 3 wt % LCh (lattice parameter a = 148 Å). The addition of LCh to the MO/W system prevents the formation of the C_D nanostructure due, presumably, to the embedment of the hydrophobic chain among the MO chains.

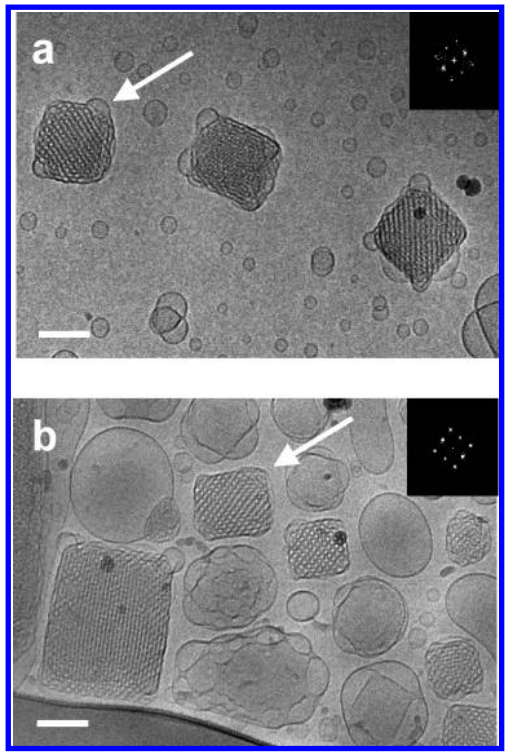

Figure 2. Cryo-TEM images of cubic phase nanoparticles (cubosomes) dispersed in the aqueous solution of PF127. Fast Fourier transformations of the domains indicated by the arrows are shown in the insets. Scale bars correspond to 100 nm.

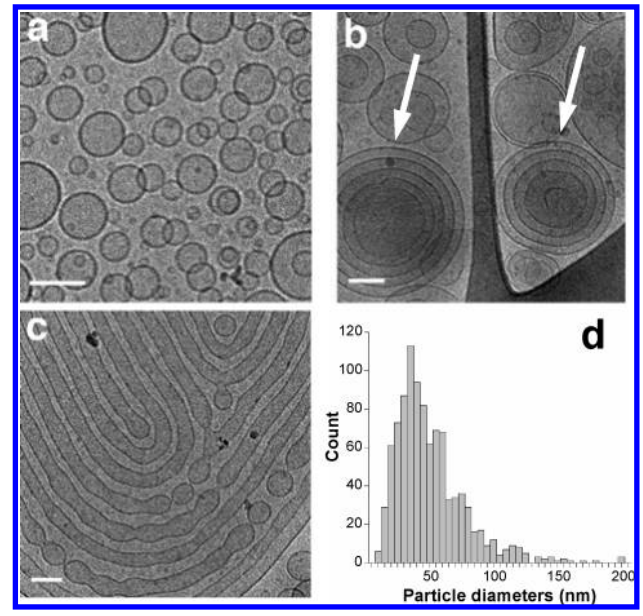

Figure 3. Cryo-TEM images of the LCh-based dispersion showing (a) unilamellar, (b) onion-like (indicated by arrows), and (c) tubular liposomes. Also shown is the unilamellar liposome size distribution (d). Scale bars correspond to 100 nm.

This increase of the hydrophobic volume fraction favors the unexpected existence of a C_G nanostructure also in excess of water.

Characterization of the Lipid Nanoparticles. The LNP dispersions were prepared via the top-down approach (see the Introduction and Experimental Methods sections). The water-to-dispersed-phase ratio (MO/W = 70/30 C_G phase plus the emulsifier) was 95/5 (w/w), while the C_G/PF127 or LCh ratio was 94/6 (w/w). It is worth mentioning that, differently from PF127 that must constitute the 6−20 wt % of the lipid fraction to properly exert its stabilizing function,[24] LCh can be used at only 1−2 wt %. Moreover, the resulting LCh-stabilized dispersions were particularly stable also at temperatures lower than those found for PF127-stabilized dispersions, presumably due to the important electrostatic contribution that prevents the coagulation. The cryo-TEM images shown in Figure 2, typical of the PF127-stabilized LNP sample, show numerous objects with the characteristic shape of cubosomes, along with the vesicular material commonly observed in previous preparations.[27,31,35,36] On the basis of repeated observations, although some cubic particles exceeding 400 nm in size were detected, this LC dispersion was found to be of low polydispersity, with cubosome dimensions estimated in the range 100−200 nm. As often reported for these kinds of dispersions, the SAXRD diffractogram was characterized by the absence of clear reflection patterns (data not shown) due to the low number of reflection planes available for each cubosome particle. Nevertheless, the retention of the LC organization of the interface after the dispersion process is strongly corroborated by the inner long-range order well distinguishable in cryo-TEM images, where water channels (bright spots) alternate to oil channels (dark matrix). Moreover, the cubic arrangement may unambiguously be inferred by the fast Fourier transform (FFT); the insets in Figure 2 show the {110} and {200} reflections from the cubosomes indicated by the arrows as seen along the [100] viewing direction of the cubic lattice. Through FFT analysis performed on a number of cubosomes, a mean lattice parameter of 136 Å was calculated, in agreement with the value previously obtained by SAXRD for the bulk C_p LC phase.

Remarkably, the use of LCh leads to an innovative method of preparation of cationic liposomes. Indeed, the dispersion process of the C_G phase in the LCh aqueous solution induces the formation of a liposome system: in this case, the cubic LC nanostructure of the original phases is completely lost. As ascertained through cryo-TEM (Figure 3), despite the sporadic occurrence of onion-like and tubular liposomes (estimated less than 0.1% of the total particle number), the LCh-stabilized LNP sample mainly consists of a homogeneous dispersion of unilamellar liposomes, characterized by a log-norm size distribution (calculated on 1000 nanoparticle measurements) with a median of about 44 nm (Figure 3d). The bilayer thickness, determined by image analysis, was found of 36 ± 3 Å, in excellent agreement with values (34−35 Å) reported elsewhere.[23]

The presence of a still structured MO interface was also proven by ^{13}C NMR relaxation. Figure 4 shows the highly resolved ^{13}C NMR spectra of the dispersions obtained in the presence of PF127 (Figure 4a) and LCh (Figure 4b) and the spin−lattice ^{13}C NMR relaxation times measured for the various carbon atoms (Figure 4c). ^{13}C NMR relaxation data demonstrate that the molecular arrangement and the time-dependent interactions are very close in the Ia3d LC phase and in the nanoparticle dispersions stabilized either by PF127 or by LCh, despite the different morphologies and topologies observed by cryo-TEM. Indeed, relaxation times are rather sensitive to modifications of the local intermolecular interactions and to molecular dynamics. Therefore, strong alterations of their values are not expected if the aggregates under analysis, though having different long-range order, share the same interfacial arrangement of the bilayer type. As a general comment, it should be noticed that moving from the polar head toward the end of the hydrophobic tail, and independently of the sample, the various carbons show similar mobilities.[37] Most remarkable is the persistence, after the dispersion process, of the local interactions in the polar-

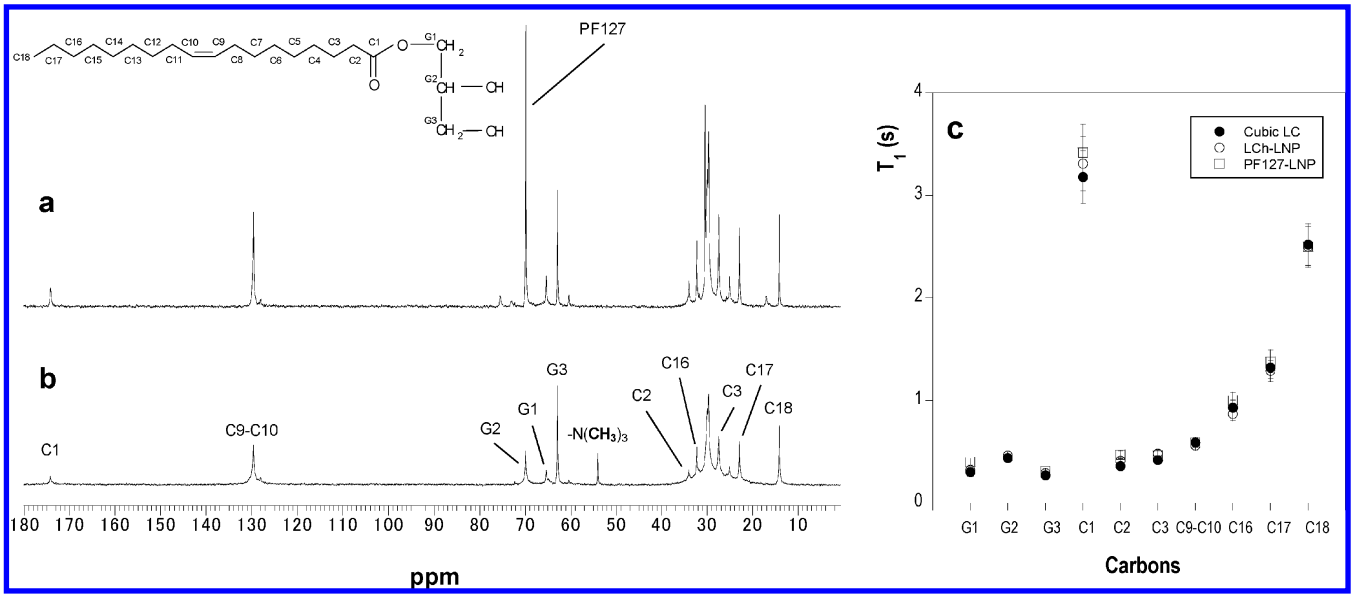

Figure 4. ^{13}C NMR data at 25 °C: (a) ^{13}C NMR spectrum of the PF127-stabilized LNPs; (b) ^{13}C NMR spectrum of the LCh-stabilized LNPs; (c) ^{13}C NMR spin−lattice relaxation times of the MO/W cubic LC phase (●, cubic LC) and of the LNPs stabilized by PF127 (□, PF127-LNP) and LCh (○, LCh-LNP). Error bars represent standard deviations.

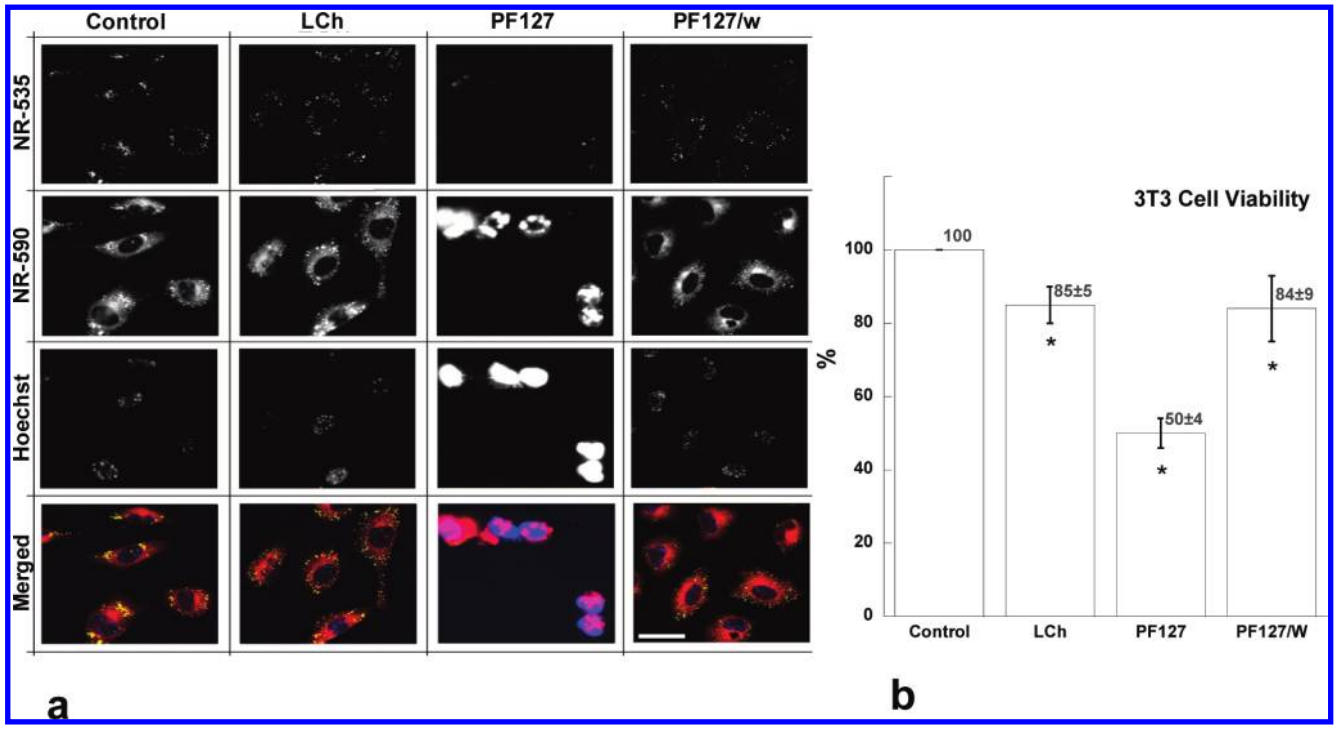

Figure 5. The 3T3 cell line. (a) Effect of the MO/W dispersions stabilized by PF127 and LCh. The panel shows the lipid droplets with NR-535, the cytoplasmic membranes with NR-590, DNA stain with Hoechst. Color images were obtained merging NR-535 (green), NR-590 (red), and Hoechst (blue). The scale bar is 30 μm. (b) Effect of the MO/W dispersions stabilized by PF127 and LCh on the cell viability of 3T3 cells as determined from Hoechst 33258 data analysis. (*) $p < 0.05$, compared to nontreated control cells.

head region as well as along the hydrophobic tail of the MO molecules which prove that the bilayer nanostructure is retained in the nanoparticles, as previously demonstrated for cubosomes and hexosomes[27] prepared via different methods.[35,36]

Biological Assays. The biological assays to evaluate the impact of these nanoparticles on the cell viability constitute an important aim of this work. Two different methodologies, image analysis and Alamar Blue assay, were applied in investigating the cytotoxicity of the LNPs. Studies were performed using three different cell lines, namely, Swiss 3T3 mouse fibroblasts (3T3), human epithelial cervical carcinoma (HeLa), and human embryonic kidney (HEK 293T) cells. Treatments were applied to actively proliferating cells (1 day after seeding).

In the case of 3T3, cell line observations were made through an inverted fluorescence microscope. Cell integrity was determined, after incubation with the nanoparticle dispersion, by staining for 15 min with the supravital fluorescent probe NR and with Hoechst 33258. NR (9-diethylamino-5*H*-benzo[α]-phenoxazine-5-one) is a fluorescent lipophilic dye characterized by a shift of emission spectrum from red to green in the presence of polar and nonpolar lipids. Cytoplasmic membranes (mostly composed of phospholipids) are stained by NR red emission

(referred to as NR-590), whereas intracellular lipid droplets (composed of apolar lipids) are stained in NR green emission (referred to as NR-535). Lipid droplets, fat-storing organelles present in all eukaryotic cells, represent an intracellular reservoir of triglycerides and esterified cholesterol.[38,39] Selective determination of cell damage was performed using Hoechst 33258 to visualize cells showing much higher nuclear fluorescence. The assay is based on the assumption that cell apoptosis is preceded by membrane permeability loss and nuclear chromatin condensation. The number of apoptotic cells and the number of healthy cells were counted. Results are expressed as the percent ratio of damaged versus total number of cells.

Results from these experiments are shown in Figure 5a. Surprisingly, LNP dispersions stabilized by PF127 show a remarkable toxicity toward the 3T3 cell line, as demonstrated by the images recorded after the treatment with both NR and Hoechst 33258 probes. The global effects of the dispersions stabilized by PF127 and LCh on the viability of 3T3 cells, determined on the basis of observations after 1 h of incubation with the different formulations, are summarized in Figure 5b. The cytotoxicity of the LNPs stabilized by PF127 is evident. Less than 60% of 3T3 cells are detectable, and most of them show apoptosis/necrosis features. In contrast, LCh-based LNP dispersions as well as the PF127 water solution affect the viability of 3T3 fibroblasts at a much lesser extent.

A different method was used to evaluate the toxicity of the dispersions stabilized by PF127 and LCh in HeLa and HEK 293T cells. Cell viability was assessed by a modified Alamar Blue assay.[40] Figure 6a shows representative images of HeLa and HEK cell lines incubated with various formulations as well as the respective controls (untreated cells). As observed in 3T3 cells, in the case of LNPs stabilized by PF127, a significant toxicity is observed, as clearly demonstrated by cell viability reported in Figure 6b and c. Both HeLa and HEK cell lines retain proliferating capacity of about 60% after incubation with PF127-stabilized LNP dispersions. Formulations stabilized by LCh, as well as the water solution of PF127, in comparison with untreated cells, did not influence cell viability notably.

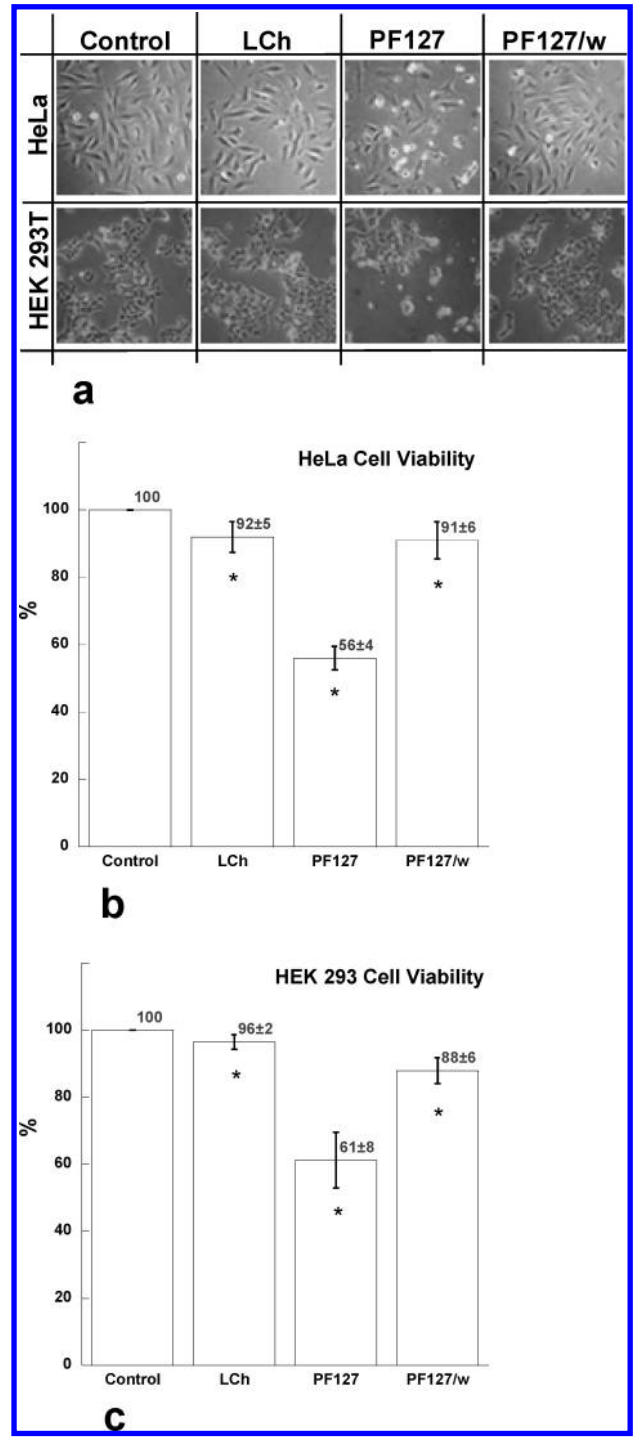

Figure 6. The HeLa and HEK 293 cell lines. (a) Morphological analysis of HeLa and HEK 293 cell lines treated with the MO/W dispersions stabilized by PF127 and LCh or PF127 alone in water (PF127/W). The scale bar is 50 μm. (b) Effect of the MO/W dispersions stabilized by PF127 and LCh on the cell viability of the HeLa cell line (Alamar Blue assay). (c) Effect of the MO/W dispersions stabilized by PF127 and LCh on the cell viability of HEK 293 cell lines (Alamar Blue assay). (*) $p < 0.05$, compared to nontreated control cells.

Discussion

The influence of the emulsifier used to stabilize the LNP dispersion is quite remarkable. Whereas PF127 allows for the formation of cubosomes as reported in previous works,[27,31,35,36] the evolution of the system's nanostructure toward unilamellar cationic liposomes upon LCh addition deserves some comments. In the latter case, the loss of the original cubic liquid crystalline matrix may be explained calling into play the effective packing parameter (P_{eff}).[10] This parameter is defined as the ratio of the volume of the surfactant tail to the product of the cross-sectional area of the surfactant polar head and the length of the surfactant hydrophobic tail. Besides the shape of the surfactant, P_{eff} is controlled by a number of factors such as the degree of hydration, the temperature, electrostatic effects, and the presence of hydrophobic/hydrophilic guest molecules.[33] Taking into account that MO LC aggregates in water show $P_{eff} \geq 1.0$,[41] while a suitable P_{eff} value for the vesicular arrangement of the bilayer is 0.5−1.0, according to our experimental result, it is clear that LCh incorporation into the MO/W system must induce a consistent decrease of P_{eff}. This logical deduction is also supported by the broadening of the L_α region and the disappearance of the C_D phase from the pseudobinary MO/W/LCh diagram (C_G has a smaller P_{eff} than C_D). Moreover, the intercalation of the short-chain LCh molecule within the MO palisade will disturb the regular arrangement of both the lipid tails and the polar head, thus increasing the bilayer flexibility. During the dispersion process, these two effects (decreased P_{eff} and increased bilayer flexibility) cooperatively act to allow for the bilayer folding toward the liposomal nanostructure. In conclusion, both the morphology and the topology of the LNPs, obtained here through the direct fragmentation of massive liquid crystalline phases, strongly depend on the chemical nature of the emulsifier. However, due to the peculiar nature of the

involved molecules, organized (bilayer) interfaces are still produced. In consideration of the huge interest of this kind of LNPs as carriers in pharmaceutical formulations, the in vitro evaluation of their biocompatibility seems to be quite important.

Independent of the incubation time used in the different assays, it is clear that PF127-stabilized LNPs induced significant toxicity. Since PF127 dissolved in water does not induce appreciable toxic effects on the three types of cell lines, toxicity should not be ascribed to PF127 itself, that in the various assays always had a concentration in the range 0.5−1.3 μmol/L (i.e., below the cmc of 40 μmol/L at 35 °C), but rather to its combination with the monoglyceride. MO, a membrane lipid, is not expected to exert any toxicity. Since MO promotes bioadhesion and internalization, it can be concluded that MO-based nanoparticles behave as a Trojan horse, thus promoting the internalization of PF127, otherwise less probable. Once inside the cells, PF127 may exert toxic activity toward mitochondrial and nuclear membranes, thus leading to cell death. Although the mechanism that drives cell apoptosis/necrosis is beyond the scope of this paper, it might be expected that this is a consequence of the amphiphilic nature of PF127. Indeed, PF127 has an HLB (hydrophilic−lipophilic balance) number around 24.[13] This implies a tendency to bury the rather large hydrophobic part (about 60 propylenoxide groups) into some biological compartment, for instance, into the mitochondrial or the nuclear membranes. This finding is in agreement with the use of various types of Pluronic (for instance, P85 of MW around 4600 and HLB in the range 12−18) to promote chemosensitization in multidrug resistant cancer cells toward antineoplastic agents.[42] In addition, a more hydrophobic variety of Pluronic, Pluronic L81 (MW 2750 and HLB 1-7), was suggested to accumulate in the cytosol, thus causing triglyceride (TG) assimilation, and, consequently, inhibition of the microsomal TG transfer protein activity.[43] In the present work, the association MO−PF127 decreases the hydrophilicity of PF127; therefore, processes similar to those reported for Pluronic P85 and L81 may occur. Although these can partly explain the experimental results, the biological mechanism by which MO/PF127 induces cell apoptosis/necrosis (in terms of involved molecular entities and specific interactions) is not clear.

Regarding the LNPs stabilized by LCh, it should be highlighted that, besides the role of MO, the bioadhesion process is likely to be functionally driven by molecular recognition between the biological membrane and the cationic polar head of the emulsifier that resembles the behavior of a charged peptide. LCh acts as a cell-penetrating peptide. This additional interaction does not produce any remarkable toxic effect, at least in a short-term treatment.

Conclusions

Due to the pressing demand for innovative pharmaceutical outcomes endowed of fine-tuned properties, it is expected that lipid based nanosystems will be widely exploited. This is due to their biocompatibility, and, more importantly, to the wide range of possible nanostructures that can modulate both drug entrapment and controlled release.

In this work, two different nanoparticle dispersions obtained from the same LC matrix have been formulated and their short-term cytotoxicity evaluated. Interestingly, the use of LCh resulted in a new and easy-to-deal-with route to prepare small unilamellar cationic liposomes that contribute to enlarge the class of liposome formulations based on single-chained surfactants. In fact, liposomes are classically obtained using double-chained surfactants (mainly phospholipids), while their counterparts based on single-chained surfactants are much less common (mixtures of cationic and anionic surfactants, known as catansome,[44] are an example). The possibility of forming MO-based vesicles in excess of water was already reported, but only highly polydisperse multilamellar large vesicles were obtained.[41,45] As a further remark, it was observed that liposomes with a size smaller than 100 nm show decreased uptake by the mononuclear phagocyte system (hence, circulate longer in the blood), thus increasing target efficiency in tumors and favoring therapeutic activity of liposomal antitumor drugs.[46] Therefore, the liposome formulation here reported can be considered as a suitable candidate for being used in this field. Indeed, LCh-based LNPs showed very low toxicity toward different cell lines after a relatively short incubation time. On the contrary, the toxicity of the PF127-stabilized LNP dispersion has been demonstrated by means of two different biological assays.

As it is included in the FDA inactive ingredients guide, MO is extensively used as an additive in food and pharmaceutical formulations. Moreover, cubosomes may definitely be regarded as the nonlamellar analogues of the liposomes. Consequently, the role of both their molecular constituents and their peculiar nanostructures in the observed cell damage can be safely excluded. Therefore, the toxic effect, even though clearly carried out by the synergistic action of MO and PF127, can be entirely ascribed to the nonionic triblock copolymer. The importance of such an observation resides on the fact that, within the variety of emulsifiers used in cubosome preparation (i.e., bile salts, casein, phospholipids,[47] and, very recently, modified cellulose[48]), PF127 is undoubtedly the most common. It deserves also noticing that PF127 is not usually considered a hazardous molecule.

This finding emphasizes the importance of establishing rigorous protocols devoted to assess the possible toxic effects of these innovative nanostructures, also when all constituents are generally recognized as safe.

Acknowledgment. MIUR-Prin 2006 (Italy), Fondazione Banco di Sardegna (Sassari, Italy), and FUSINT project with the National Research Council (CNR, Italy) are acknowledged for financial support. Sigrid Bernstorff and Michael Rappolt, Elettra Synchrotron, Trieste, Italy, are thanked for the essential assistance during SAXRD experiments (project 2007585). Electron Microscopy was performed in the Technion Laboratory for Advanced Microscopy of Soft Matter, supported by the Technion Russell Berrie Nanotechnology Institute (RBNI). Thanks are due to Tommy Nylander of the Physical Chemistry 1 Department, Lund, for making available several preliminary cryo-TEM characterizations and to Gavin Mountjoy of the Department of Chemical Science, Cagliari University, for fruitful discussions concerning the FFT analysis.

References and Notes

(1) Panessa-Warren, B. J.; Warren, J. B.; Wong, S. S.; Misewich, J. A. *J. Phys.: Condens. Matter* **2006**, *18*, S2185.
(2) Stone, V.; Donaldson, K. *Nat. Nanotechnol.* **2006**, *1*, 23.
(3) Nel, A.; Xia, T.; Madler, L.; Li, N. *Science* **2006**, *311*, 622.
(4) Oberdorster, G.; Stone, V.; Donaldson, K. *Nanotoxicology* **2007**, *1*, 2.
(5) Diaz, B.; Sanchez-Espinel, C.; Arruebo, M.; Faro, J.; deMiguel, E.; Magadan, S.; Yague, C.; Fernandez-Pacheco, R.; Ibarra, M. R.; Santamaria, J.; Gonzalez-Fernandez, A. *Small* **2008**, *4*, 2025.
(6) Zhang, H.; Wang, D.; Butler, R.; Campbell, N. L.; Long, J.; Tan, B.; Duncalf, D. J.; Foster, A. J.; Hopkinson, A.; Taylor, D.; Angus, D.; Cooper, A. I.; Rannard, S. P. *Nat. Nanotechnol.* **2008**, *3*, 506.
(7) Berti, D.; Barbaro, P.; Bucci, I.; Baglioni, P. *J. Phys. Chem. B* **1999**, *103*, 4916.
(8) Marchi-Artzner, V.; Lehn, J.-M.; Kunitake, T. *Langmuir* **1998**, *14*, 6470.

(9) Sideratou, Z.; Foundis, J.; Tsiourvas, D.; Nezis, I. P.; Papadimas, G.; Paleos, C. M. *Langmuir* **2002**, *18*, 5036.
(10) Angius, R.; Murgia, S.; Berti, D.; Baglioni, P.; Monduzzi, M. *J. Phys.: Condens. Matter* **2006**, *18*, S2203.
(11) Ganem-Quintanar, A.; Quintanar-Guerrero, D.; Buri, P. *Drug Dev. Ind. Pharm.* **2000**, *26*, 809.
(12) Malmsten, M. *Surfactants and Polymers in Drug Delivery*; Marcel Dekker: New York, 2002.
(13) Evans, D. F.; Wennerstrom, H. *The colloidal domain: where Physics, Chemistry, Biology, and Technology meet*; VCH: New York, 1994.
(14) Hyde, S.; Andersson, S.; Larsson, K.; Blum, Z.; Landh, T.; Lidin, S.; Ninham, B. W. *The Language of Shape*; Elsevier: Amsterdam, The Netherlands, 1997; Chapters 1−5.
(15) Vinardell, M. P. *Toxicol. Sci.* **2005**, *88*, 285.
(16) Sager, T. M.; Porter, D. W.; Robinson, V. A.; Lindsley, W. G.; Schwegler-Berry, D. E.; Castranova, V. *Nanotoxicology* **2007**, *1*, 118.
(17) Barauskas, J.; Johnsson, M.; Tiberg, F. *Nano Lett.* **2005**, *5*, 1615.
(18) Larsson, K. *Nature* **1983**, *304*, 664.
(19) Larsson, K. *Curr. Opin. Colloid Interface Sci.* **2000**, *5*, 64.
(20) Hyde, S. T. *J. Phys. Chem.* **1989**, *93*, 1458.
(21) Hyde, S. T.; Andersson, S.; Ericsson, B.; Larsson, K. *Z. Kristallogr.* **1984**, *168*, 213.
(22) Caboi, F.; Nylander, T.; Razumas, V.; Talaikyte, Z.; Monduzzi, M.; Larsson, K. *Langmuir* **1997**, *13*, 5476.
(23) Murgia, S.; Lampis, S.; Angius, R.; Berti, D.; Monduzzi, M. *J. Phys. Chem. B* **2009**, *113*, 9205.
(24) Barauskas, J.; Johnsson, M.; Joabsson, F.; Tiberg, F. *Langmuir* **2005**, *21*, 2569.
(25) Ljusberg-Wahren, H.; Nyberg, L.; Larsson, K. *Chim. Oggi* **1996**, *14*, 40.
(26) Neto, C.; Aloisi, G.; Baglioni, P.; Larsson, K. *J. Phys. Chem. B* **1999**, *103*, 3896.
(27) Monduzzi, M.; Ljusberg-Wahren, H.; Larsson, K. *Langmuir* **2000**, *16*, 7355.
(28) Nakano, M.; Sugita, A.; Matsuoka, H.; Handa, T. *Langmuir* **2001**, *17*, 3917.
(29) Spicer, P. T.; Hayden, K. L.; Lynch, M. L.; Ofori-Boateng, A.; Burns, J. L. *Langmuir* **2001**, *17*, 5748.
(30) Landh, T.; Larsson, K. U.S. Patent 5,531,925, 1996.
(31) Popescu, G.; Barauskas, J.; Nylander, T.; Tiberg, F. *Langmuir* **2007**, *23*, 496.
(32) Talmon, Y. Seeing Giant Micelles by Cryogenic-Temperature Transmission Electron Microscopy (Cryo-TEM). In *Giant Micelles*; Zana, R., Kaler, E. A., Eds.; CRC Press: New York, 2007; p 163.
(33) Caboi, F.; Amico, G. S.; Pitzalis, P.; Monduzzi, M.; Nylander, T.; Larsson, K. *Chem. Phys. Lipids* **2001**, *109*, 47.
(34) Landh, T. *J. Phys. Chem.* **1994**, *98*, 8453.
(35) Gustafsson, J.; Ljusber-Wahren, H.; Almgren, M.; Larsson, K. *Langmuir* **1997**, *13*, 6964.
(36) Gustafsson, J.; Ljusberg-Wahren, H.; Almgren, M.; Larsson, K. *Langmuir* **1996**, *12*, 4611.
(37) Murgia, S.; Caboi, F.; Monduzzi, M. *Chem. Phys. Lipids* **2001**, *110*, 11.
(38) Diaz, G.; Melis, M.; Batetta, B.; Angius, F.; Falchi, A. M. *Micron* **2008**, *39*, 819.
(39) Diaz, G.; Batetta, B.; Sanna, F.; Uda, S.; Reali, C.; Angius, F.; Melis, M.; Falchi, A. M. *Histochem. Cell Biol.* **2008**, *129*, 611.
(40) Fields, R. D.; Lancaster, M. V. *Am. Biotechnol. Lab.* **1993**, *11*, 48.
(41) Borné, J.; Nylander, T.; Khan, A. *Langmuir* **2001**, *17*, 7742.
(42) Kabanov, A.; Batrakova, E.; Alakhov, V. *Adv. Drug Delivery Rev.* **2002**, *54*, 759.
(43) Fatma, S.; Yakubov, R.; Anwar, K.; Hussain, M. M. *J. Lipid Res.* **2006**, *47*, 2422.
(44) Yang, Y.-M.; Wu, K.-C.; Huang, Z.-L.; Chang, C.-H. *Langmuir* **2008**, *24*, 1695.
(45) Ferreira, D. A.; Bentley, M. V. L. B.; Karlsson, G.; Edwards, K. *Int. J. Pharm.* **2006**, *310*, 203.
(46) Nagayasu, A.; Uchiyama, K.; Kiwada, H. *Adv. Drug Delivery Rev.* **1999**, *40*, 75.
(47) Johnsson, M.; Barauskas, J.; Tiberg, F. *J. Am. Chem. Soc.* **2005**, *127*, 1076.
(48) Uyama, M.; Nakano, M.; Yamashita, J.; Handa, T. *Langmuir* **2009**, *25*, 4336.

JP9098655